



Ultrafast reversible phase engineering in MoTe₂ thin film via polaron formation

Ji-Hee Kim¹ · Gunnar Schönhoff^{2,3} · Michael Lorke² · Tim O. Wehling^{2,3} · Ki-Ju Yee⁴

Received: 11 April 2024 / Accepted: 25 April 2024
© The Author(s) 2024

Abstract

The emergence of various polymorphs in two-dimensional transition metal dichalcogenides provides an opportunity for robust phase engineering by temperature, strain, laser irradiation, and external charge doping (Keum in *Nat. Phys.* 11:482, 2015; Song in *Nano Lett.* 16:188, 2016; Cho in *Science* 349:625, 2015; Kim in *Nano Lett.* 17:3363, 2017). This provides means to develop homojunction of metal–semiconductor, enhance mobility, reduce contact resistance, and observe novel quantum critical phenomena in mesoscopic systems. The rich physics paves the way for ultrafast light-induced switching/memory devices and optical data processing in optoelectronics. However, the fundamental temporal evolution of the laser-driven phase transformation, in particular regarding heat and charge carriers, remains elusive. We report an ultrafast reversible structural transformation in MoTe₂ by coherent phonon dynamics through polaron formation at room temperature. At a high photon density, the generated coherent phonons are coupled with excitons to form polarons. The strong exciton–phonon coupling disturbs and dephases the coherent phonons of the semiconducting 2H phase in MoTe₂, and generates lattice distortions to further stabilize new coherent phonons of the metallic 1T' phase, manifested by the emergence of the corresponding phonons in each phase. This structural transformation is fully reversible within a few picoseconds by switching on/off the laser. The nonlinear response of the phonon intensity to the excited carrier density in the intermediate region indicates a gradual structural transformation through coexisting 2H and 1T' phases.

Keywords MoTe₂ · Polaron formation · Phase transition · Coherent phonon

1 Introduction

Electron–phonon coupling in condensed matter physics leads to novel phenomena such as superconductivity, Joule heating, Peierls instability, and magnetoresistance [5–8]. This interaction, when considered in a strongly coupled regime, provokes local and cooperative lattice distortions, which tend to be rearranged with the generated exciton density. The van der Waals (vdW) layered materials, with a

strong Coulomb interaction, provide a large exciton binding energy (0.3–1 eV) in a monolayer [9–11], although these values are scaled down to less than 100 meV by charge screening in a thin film. In addition to the large exciton binding energy, excitons are easily localized by defects or impurities [12–15]. Excitons can be also localized by light illumination, and thus the probability of coupling between localized excitons and phonons is enhanced at a high optical density, eventually inducing an excitonic polaron formation [16, 17]. Such mesoscopic phenomenon is further complicated by the fluence and energy of the laser, let alone the phonon dynamics involving radiative/non-radiative energy dissipations with heat and charge carriers [18].

Coherent phonon spectroscopy via femtosecond pump-probe techniques enables direct measurement of time-resolved lattice vibrations and investigate their interactions with charge, spin, and lattice degrees of freedom in solids [19–21]. Transition metal dichalcogenides (TMDs), consisting of a metal layer sandwiched by two chalcogen top and bottom layers, provide an additional degree of freedom

✉ Ji-Hee Kim
kimjihee@pusan.ac.kr

¹ Department of Physics, Pusan National University, Busan, Republic of Korea

² Institut für Theoretische Physik, Universität Bremen, Ott-Hahn-Allee 1, Bremen, Germany

³ Bremen Center for Computational Materials Science, Universität Bremen, Am Fallturm, 1a, Bremen, Germany

⁴ Department of Physics, Chungnam National University, Daejeon, Republic of Korea

in the atomic rearrangement. This permits various types of polymorphs, which are easily engineered by external parameters [1–4]. Nevertheless, an information on the dynamical behavior of the phase transformation is lacking. In this study, we report picosecond-scale reversible phase transformations in MoTe₂ from the 2H to the 1T' phase using coherent phonon dynamics, induced by the strong electron–phonon coupling through an excitonic polaron formation without a heating effect. All measurements are performed at room temperature.

2 Experiments and discussion

2.1 Time-domain coherent phonon spectroscopy

To generate and detect coherent vibrations of the lattice, the femtosecond pump–probe technique was employed at room temperature. The pump pulse was delivered by a mode-locked Ti:sapphire oscillator with a pulse duration of 60 fs at an excitation energy of 1.57 eV (790 nm) and repetition rate of 400 kHz. In the path of the pump, a scanning shaker (APE Scan Delay, Germany) was installed to mechanically generate the optical time delay. The probe pulse was derived from the same laser, maintaining a weaker intensity of 95% than the pump pulse. The focused spot's diameter of the pump on the sample was approximately 5 μm, while that of the probe was slightly smaller. The differential transmittance was measured using the probe pulse as a function of the delay time, with respect to the pump pulse, and pump fluence from 24.8 to 918 μJ/cm².

2.2 Sample preparation and optical characterization

A commercial 2H-MoTe₂ purchased from HQ Graphene, Netherlands was exfoliated using a standard taping method. After the exfoliation, a flake of approximately 4–5 layers was transferred onto a quartz substrate, and placed under vacuum during the measurements. The sample was retained without changing the morphology during the pulse laser illumination. After the removal of the laser, the sample was recovered to the 2H phase. The excitons were observed by measuring the absorbance (V-670 UV–VIS–NIR spectrophotometer, JASCO, Germany).

2.3 Change of the total energy

We performed density functional theory calculations using the Quantum Espresso package [27], with the generalized gradient approximation pseudopotentials. The lattice parameters of both 2H and 1T' phases were set to 3.53 Å, and the structures were fully relaxed. We used *k*-meshes of 36 × 36

× 1 for the 2H phase and 24 × 24 × 1 for the 2 × 2 supercell of the 1T' phase. We obtained the total energies of the 2H (E_{2H}^0) and 1T' ($E_{1T'}^0$) phases in the ground state, i.e., without optical excitations.

The excitation-induced change in the total energy δE is calculated using:

$$\delta E^{\text{h,e}}(\mu^{\text{h,e}}) = \int_0^{\mu^{\text{h,e}}} d\epsilon \rho(\epsilon) \epsilon, \quad (1)$$

for both holes and electrons with chemical potentials $\mu^{\text{h,e}}$ and density of states ρ of the corresponding phase. The total energy change is then given by $\delta E(n) = \delta E^e(n) + \delta E^h(n)$, where the number of excited carriers:

$$n^{\text{h,e}}(\mu^{\text{h,e}}) = \int_0^{\mu^{\text{h,e}}} d\epsilon \rho(\epsilon), \quad (2)$$

is required to satisfy $n^h = n^e$.

Coherent phonons (or in-phase phonons) are generated by irradiating a pulsed laser to the sample with an input pump-pulse duration shorter than the phonon period [22, 23]. We used a semiconducting 2H-MoTe₂ thin film (4–5 layers) to generate coherent phonons using a pump–probe technique with a pump pulse (duration of 60 fs, central wavelength of 780 nm, and repetition rate of 400 kHz; see also Methods and Extended Data Fig. 1) for two different pump fluencies of 24.9 μJ·cm⁻² and 918 μJ·cm⁻² (Fig. 1). The differential transmittance change $\Delta T/T$ (Fig. 1a) abruptly peaks at zero time delay and exponentially decreases in the subsequent time delay, which is attributed to the change of the photoexcited carrier density. The increasing maximum of $\Delta T/T$ with the fluence is attributed to the increase of the excited carrier density (see also Extended Data Fig. 2). In addition to this large electronic contribution, a weakly decaying oscillatory signal originating from the coherent phonons is clearly visible owing to the large amplitude of oscillation of $\sim 10^{-3}$ near zero delay. This change is still visible but less apparent at a low pump fluence. By subtracting the exponential decay component, we can clearly visualize such oscillatory behaviors of coherent phonons even at a low pump fluence (Fig. 1b).

At a higher fluence, the oscillatory signal clearly reveals a beating pattern with a large amplitude, indicating that the coherent lattice vibrations consist of different vibrating frequencies. By performing a fast Fourier transform of the time-domain coherent lattice vibrations, we obtain various phonon modes, as shown in Fig. 1c. Three peaks at 5.22, 4.99, and 4.83 THz (173, 166, and 163 cm⁻¹) are well matched with the A_{1g} mode of the semiconducting 2H-MoTe₂, and B_g and A_g modes of the metallic 1T'-MoTe₂, respectively [24] (see also Extended Data Fig. 3a). At a lower fluence, a long-lived oscillation is exclusively

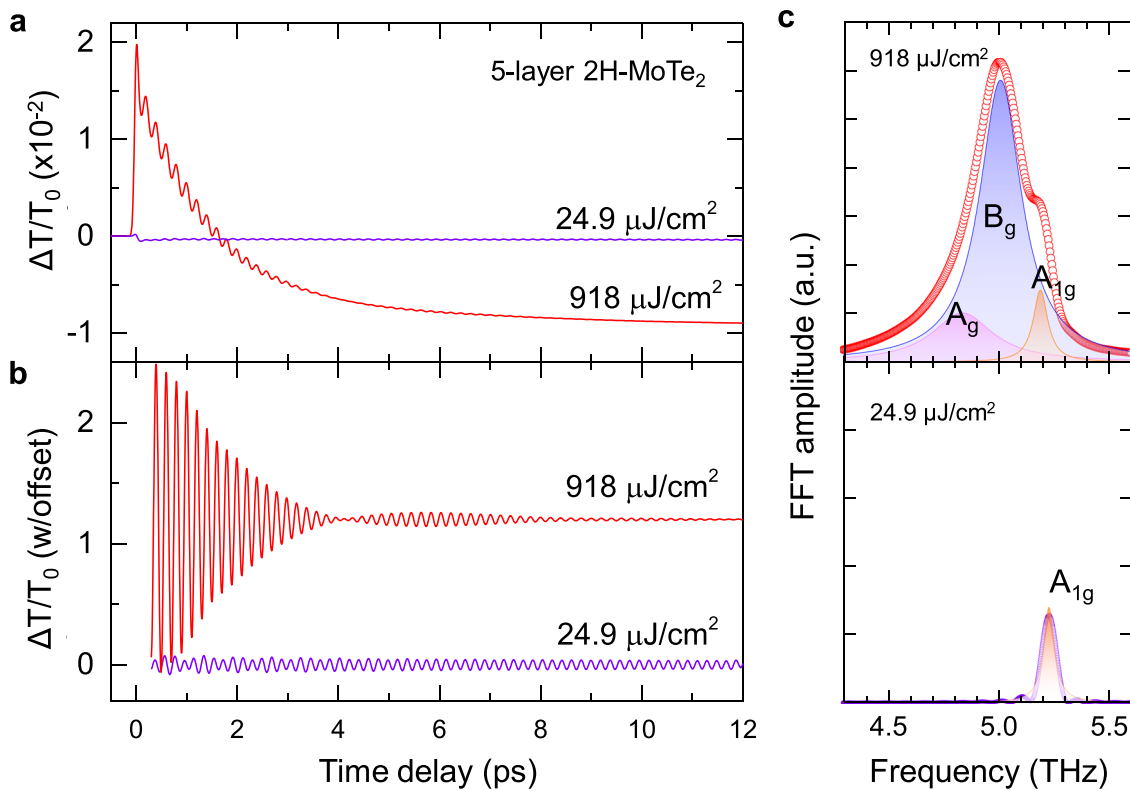


Fig. 1 Differential transmittance change for 5-layer 2H-MoTe₂ film at 780 nm. **a** Differential transmittance at 24.87 and 918 $\mu\text{J}/\text{cm}^2$ fluences. **b** Coherent phonon oscillation data in time domain, extracted from (a) by removing the exponential decay component. **c** Fast Fourier transform (FFT) spectra. At higher excitation fluence (top), three

frequencies deconvoluted, whereas a single peak appeared at lower fluence (bottom). The peak at ~ 5.22 THz (173 cm^{-1}) corresponds to A_{1g} mode in the semiconducting 2H phase, while the two peaks at 4.99 THz (166 cm^{-1}) and 4.83 THz (163 cm^{-1}) correspond to B_g and A_g modes in the metallic 1T'-phase, respectively

observed in Fig. 1b, corresponding to the coherent A_{1g} mode (173 cm^{-1}) of 2H-MoTe₂. This strongly indicates that, at a high fluence, the structural transformation evolves with time from a semiconducting 2H to a new metallic 1T' phase.

Excitons are simultaneously generated with the coherent phonons by the pump pulse, which is confirmed by the absorbance spectrum at room temperature of the 2H-MoTe₂ phase (see Extended Data Fig. 3b). At a high pump fluence, the exciton density is high and starts interacting with the coherent phonons, leading to a formation of polarons [17]. This disturbs the coherent phonons, dephases the coherency of the phonons, and consequently induces new coherent phonons at different phases. A metallic 1T'-MoTe₂ film is stable at a high carrier density [1]. Therefore, the structural evolution from a semiconducting 2H phase to a metallic 1T' phase at a high fluence appears to occur naturally. This will be further discussed in the following section.

To systematically investigate the phase transformation, the pump fluence was varied from 24.9 to 918 $\mu\text{J}\cdot\text{cm}^{-2}$, and subsequently reduced to 24.9 $\mu\text{J}\cdot\text{cm}^{-2}$. When the pump fluence exceeds approximately 100 $\mu\text{J}\cdot\text{cm}^{-2}$, the single peak of the A_{1g} phonon mode of 2H-MoTe₂ (5.22 THz) at a

low pump fluence is no longer stable and slightly softened (Fig. 2a and b). In addition, new peaks near the A_g and B_g modes emerge, representing the characteristics of the metallic 1T'-MoTe₂. These peaks remain stable until the highest fluence used in this experiment. The single peak of the A_{1g} phonon mode of the original 2H-MoTe₂ is fully recovered at a low fluence. A similar trend was observed in the amplitude variance (Fig. 2c). Notably, the new phase emerges when the excited carrier density exceeds approximately $4 \times 10^{14}\text{ cm}^{-2}$. This photoexcited carrier density is similar with an externally injected carrier density to induce a phase transition [4].

Furthermore, the thermal effect owing to the laser illumination is negligible in this experiment. The phonon softening of the 2H phase at a high pump fluence of 918 $\mu\text{J}\cdot\text{cm}^{-2}$ is 1.3 cm^{-1} (Fig. 2b), which is a negligible temperature increment determined by the temperature coefficient of 0.8 meV/K [25]. Stable phonons of the 1T' phase (B_g : 166 cm^{-1} and A_g : 163 cm^{-1}) are obtained at a fluence of 918 $\mu\text{J}\cdot\text{cm}^{-2}$, whose positions are equal to those observed at room temperature, thus confirming the negligible thermal effect in our case [26]. The thermal effect is further evaluated at a higher repetition rate (80 MHz) of the pump pulse.

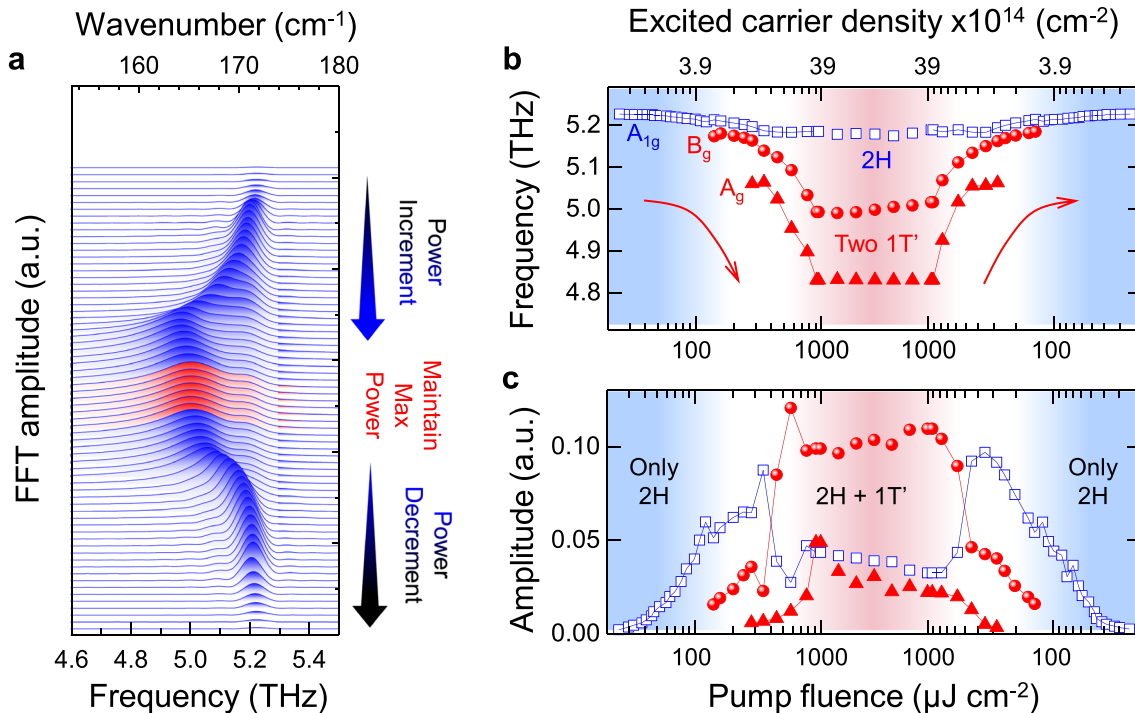


Fig. 2 Evolution of phonon modes during the photo-induced phase transformation. **a** FFT spectra with the increase and decrease of the pump fluence. **b** Variation of the phonon frequencies with the pump

fluence. **c** FFT amplitude as a function of the pump fluence. At the high-power regime, two phases (2H and 1T') emerge. With the decrease of the power, the 2H phase is fully recovered

In this case, the heat is accumulated in the sample, eventually burning the sample at a significantly lower fluence (see Extended Data Fig. 4 and Supplementary Note).

Wavelet transform (WT) can be employed to analyze amplitudes and frequencies of lattice vibrations and visualize their temporal evolution. The Gaussian function is used as the basic window function:

$$f(t) = \frac{1}{\omega\sqrt{2\pi}} e^{-\frac{(t-t_i)^2}{2\omega^2}},$$

where t_i and ω are the position and width of the Gaussian function in the time domain ($\omega = 1$ ps in this study), respectively. The Gaussian function multiplied by the oscillatory signal in Fig. 1b is further Fourier-transformed to obtain the WT mapping, as shown in Fig. 3a and b. The obtained phonon frequencies correspond to the Fourier transform data, shown in the top panels, except the broader spectral width. At the high-fluence regime, transient frequencies and amplitudes apparently emerged, compared to a monotonic frequency at the low-fluence regime. Distinct two-phonon modes at the semiconducting A_{1g} (5.22 THz) and metallic A_g (4.83 THz) were apparent at a later time delay (~5 ps), although two-phonon modes at an early time delay (~2 ps) were dubious with a broad spectral width (Fig. 3b). After ~5 ps, these two-phonon modes decay, and the metallic

B_g (4.99 THz) evolves with a further delay (see Extended Data Fig. 5). This assures that the structural transformation from the semiconducting to the metallic phase occurs in an ultrafast picosecond time-scale.

A coherent phonon oscillation at a low pump fluence is persistent without a considerable decay even with a long delay time, while the large amplitude of the coherent phonons at a high pump fluence rapidly decays with the delay time (Fig. 1b). To obtain dynamic quantities of the coherent phonons, i.e., dephasing time, each oscillation with different fluences is fitted to a sum of damped oscillations:

$$y = A_n \times \sin(\Omega_n(t_n - \varphi_n)) \times e^{-t/\tau_n},$$

where n denotes the number of phonon modes depending on the fluence, A represents the amplitude, Ω represents the phonon frequency, t represents time, φ represents phase, and τ represents the dephasing time. The extracted dephasing time τ is plotted as a function of the fluence for each phonon mode (Fig. 3c and d). At a low fluence, the 2H phase is dominant with a dephasing time of 20 ± 5 ps. When the fluence exceeds approximately $100 \mu\text{J cm}^{-2}$, the dephasing time decreases and reaches the value of approximately 2.5 ps at the highest fluence. Moreover, the newly emerging coherent phonons of the B_g and A_g modes in the 1T'-phase reveal faster dephasing times ($\sim 2 \pm 0.5$ ps and ~ 0.5 ps,

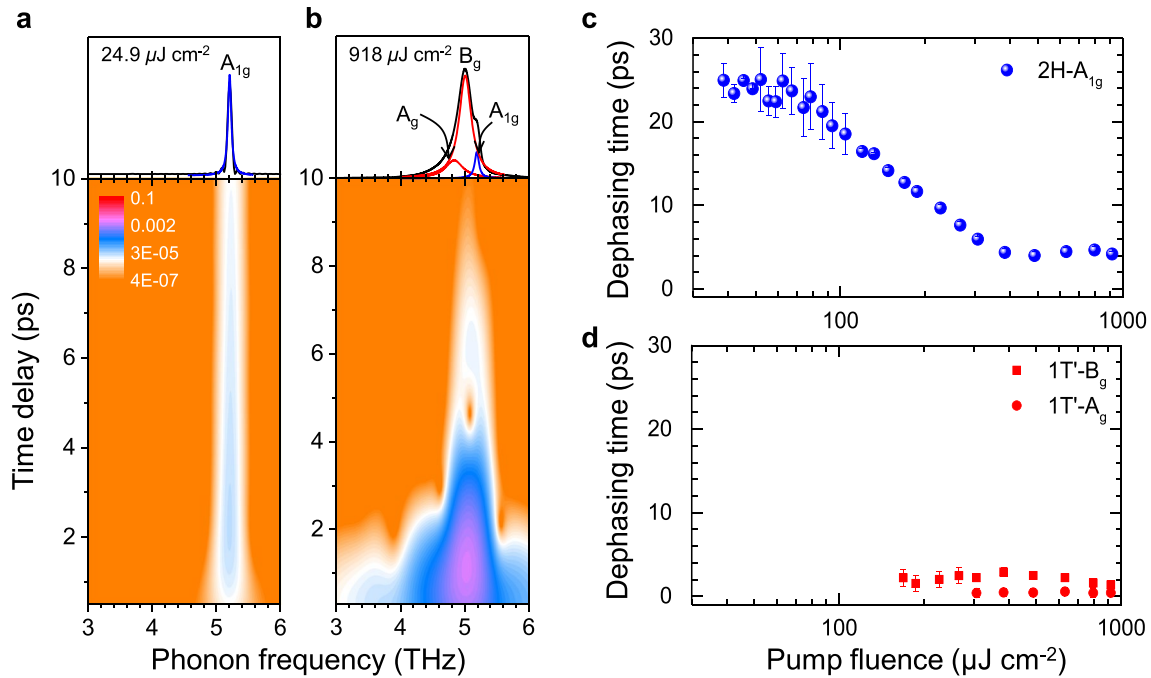


Fig. 3 Time–frequency analysis with pump fluence. **a** and **b** WT chronograms of Fig. 1a and b, respectively. The top panels represent the normal Fourier transform spectra. **c** Dephasing time as a func-

tion of the pump fluence for the coherent A_{1g} phonon mode in the 2H phase, and **d** a similar plot for the two coherent B_g and A_g phonon modes in the 1T' phase

respectively) in the high-fluence regime, independent of the fluence. This suggests that the coherency of lattice vibrations is perturbed by the photoexcited electron–hole pairs at a high density within a picosecond time-scale.

An emergence of polarons is expected when the photoexcited electron–hole pairs moving in a crystal are coupled to phonons [17]. At a low pump fluence, the phonon intensity associated with the 2H-MoTe₂ phase is linearly proportional to the excited carrier density up to $4 \times 10^{14} \text{ cm}^{-2}$ (Fig. 4a). In this regime (blue box), the phonon density of the 2H phase increases linearly with the exciton density; however, the exciton density would not be sufficient to dephase the motion of the coherent phonons, thus still preserving the stable 2H-MoTe₂ phase. In the intermediate regime (white box), the photoexcited carrier density exceeds $4 \times 10^{14} \text{ cm}^{-2}$, leading to a strong exciton–phonon coupling to form exciton polarons. This strong exciton–phonon coupling disturbs and dephases the coherent phonons of the 2H phase with a delay time. The dephased phonons subsequently create new coherent phonons of the 1T' phase, which are stable at a high carrier density. Consequently, the 2H and 1T' phases initially coexist, as already demonstrated in Fig. 2b. The coherent phonons corresponding to the 1T' phase become stable and dominant (Fig. 2c) when the exciton density exceeds $9 \times 10^{14} \text{ cm}^{-2}$. The 1T' phonon density is represented by another linear slope (Fig. 4a).

The slope of the phonon density in the intermediate regime can be expressed as a sum of the slopes of the 2H and 1T' phases: $S_{\text{int}} = (1 - x) S_{2\text{H}} + x S_{1\text{T}'}$, where S_{α} represents the slope of the α phase and x represents the composition of the 1T' phase expressed in percentages. For known slopes at each point, we obtain x as a function of the exciton density (Fig. 4b). Our analysis clearly demonstrates the phase transformation from the 2H to the 1T' structure with coexistence in the intermediate region. In addition, the change in the total energy is calculated as a function of the photogenerated carrier density (see Methods section). We estimate the total energy difference between the 2H and 1T' phases, as shown in Fig. 4c. The 2H phase is preferred at a low optical carrier density, while the 1T' phase becomes more stable at a carrier density above approximately 10^{14} cm^{-2} of the MoTe₂ monolayer. This carrier density is in agreement with the experimentally observed onset of the transition between the two phases in 4–5 layers of a MoTe₂ film (Fig. 2b). The control of the exciton–phonon coupling amplitude accompanying lattice distortions is the key to induce the dephasing of coherent vibrations. The dephasing time is ultrashort with a time-scale of a few picoseconds. The phase transition is fully reversible within several picoseconds by simply removing the laser illumination, thus recovering the semiconducting 2H phase from the metallic 1T' phase. This paves the way for applications of van der Waals layered materials for

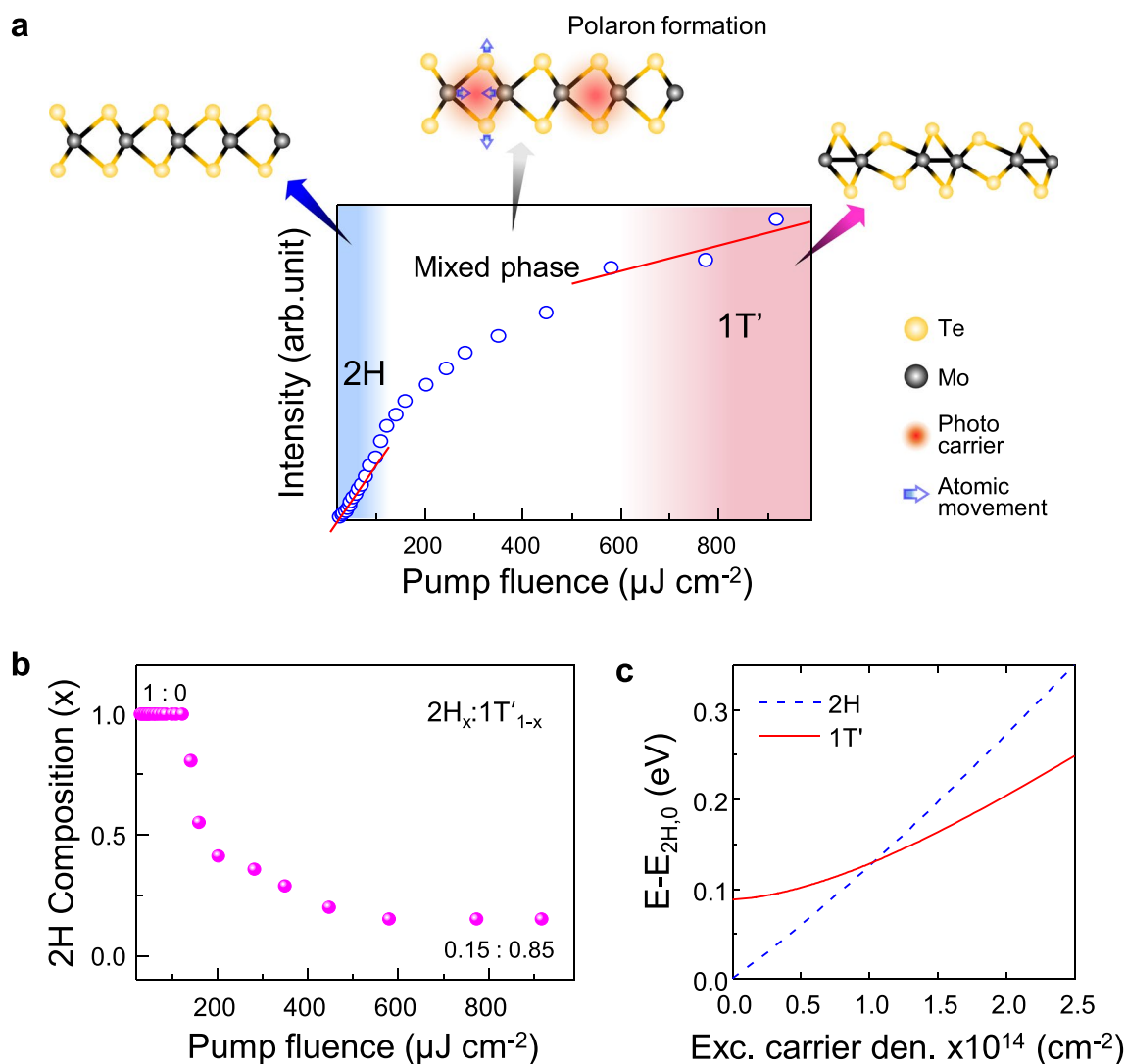


Fig. 4 Evolution of the lattice distortion through a polaron formation. **a** FFT intensity of the time-domain oscillation signal as a function of the excited carrier density. **b** Composition variation from the semiconducting 2H phase to the metallic 1T' phase with the excited carrier density.

c Total energy per Mo atom depending on the density of photoexcited electrons and holes for the 2H and 1T' phases, with respect to the energy $E_{2\text{H},0}$ of the 2H phase in the absence of any photoexcited carriers. All values are given per one MoTe₂ layer

ultrafast light-induced switching/memory devices and optical data processing in optoelectronics.

3 Conclusion

We investigated ultrafast reversible structural transformations in MoTe₂ thin films at room temperature. By employing a femtosecond pump–probe technique, we have successfully demonstrated that high photon density can induce a rapid transition from the semiconducting 2H phase to the metallic 1T' phase in MoTe₂. This transition is attributed to the strong exciton-phonon coupling that leads to polaron formation, significantly altering the

lattice structure without thermal effects. We reveal that the structural transformation is fully reversible within a few picoseconds by simply turning the laser on or off, highlighting the role of polarons in facilitating this rapid phase change. We provide crucial insights into the temporal evolution of phase transitions in transition metal dichalcogenides (TMDs), which are vital for developing future optoelectronic devices. The ability to reversibly and rapidly change the structural phase of MoTe₂ paves the way for the creation of ultrafast light-induced switching/memory devices and offers new avenues for optical data processing in optoelectronics. This results not only advance the understanding of the fundamental structural properties of TMDs but also open up possibilities for their

application in high-speed, low-energy consumption electronic and photonic devices.

Supplementary Information The online version contains supplementary material available at <https://doi.org/10.1007/s40042-024-01077-9>.

Acknowledgements This work was supported by a 2-Year Research Grant of Pusan National University. We thank T.Y.J. at Chungnam National University for his technical support in pump-probe measurements.

Open Access This article is licensed under a Creative Commons Attribution 4.0 International License, which permits use, sharing, adaptation, distribution and reproduction in any medium or format, as long as you give appropriate credit to the original author(s) and the source, provide a link to the Creative Commons licence, and indicate if changes were made. The images or other third party material in this article are included in the article's Creative Commons licence, unless indicated otherwise in a credit line to the material. If material is not included in the article's Creative Commons licence and your intended use is not permitted by statutory regulation or exceeds the permitted use, you will need to obtain permission directly from the copyright holder. To view a copy of this licence, visit <http://creativecommons.org/licenses/by/4.0/>.

References

1. D.H. Keum et al., Bandgap opening in few-layered monoclinic MoTe₂. *Nat. Phys.* **11**, 482 (2015)
2. S. Song et al., Room temperature semiconductor-metal transition of MoTe₂ thin films engineered by strain. *Nano Lett.* **16**, 188 (2016)
3. S. Cho et al., Phase patterning for ohmic homojunction contact in MoTe₂. *Science* **349**, 625 (2015)
4. S. Kim et al., Long-range lattice engineering of MoTe₂ by 2D electride. *Nano Lett.* **17**, 3363 (2017)
5. D. Reznik et al., Electron-phonon coupling reflecting dynamic charge inhomogeneity in copper oxide superconductors. *Nature* **440**, 1170 (2006)
6. K.H. Baloch, N. Voskanyan, M. Bronsgeest, J. Cumings, Remote Joule heating by a carbon nanotube. *Nat. Nanotech.* **7**, 316 (2012)
7. M.P. Jiang et al., The origin of incipient ferroelectricity in lead telluride. *Nat. Commun.* **7**, 12291 (2016)
8. D. Edwards, Ferromagnetism and electron-phonon coupling in the manganites. *Adv. Phys.* **51**, 1259 (2002)
9. K.F. Mak et al., Tightly bound trions in monolayer MoS₂. *Nat. Mater.* **12**, 207 (2013)
10. J. Yang et al., Robust excitons and trions in monolayer MoTe₂. *ACS Nano* **9**, 6603 (2015)
11. A. Mitoglu et al., Optical investigation of monolayer and bulk tungsten diselenide (WSe₂) in high magnetic fields. *Nano Lett.* **15**, 4387 (2015)
12. M. Amani et al., Near-unity photoluminescence quantum yield in MoS₂. *Science* **350**, 1065 (2015)
13. S. Tongay et al., Defects activated photoluminescence in two-dimensional semiconductors: interplay between bound, charged, and free excitons. *Sci. Rep.* **3**, 2657 (2013)
14. M. Palummo, M. Bernardi, J.C. Grossman, Exciton radiative lifetimes in two-dimensional transition metal dichalcogenides. *Nano Lett.* **15**, 2794 (2015)
15. A. Srivastava et al., Optically active quantum dots in monolayer WSe₂. *Nat Nano* **10**, 491 (2015)
16. A. Thilagam, Excitonic polarons in low-dimensional transition metal dichalcogenides. *Physica B* **464**, 44 (2015)
17. C. Chen et al., Emergence of interfacial polarons from electron-phonon coupling in graphene/h-BN van der waals heterostructures. *Nano Lett.* **18**(2), 1082–1087 (2018)
18. M.-F. Lin et al., Ultrafast non-radiative dynamics of atomically thin MoSe₂. *Nat. Commun.* **8**, 1745 (2017)
19. M. Eichberger et al., Snapshots of cooperative atomic motions in the optical suppression of charge density waves. *Nature* **468**, 799 (2010)
20. K.W. Kim et al., Ultrafast transient generation of spin-density-wave order in the normal state of BaFe₂As₂ driven by coherent lattice vibrations. *Nat. Mater.* **11**, 497 (2012)
21. A. Cavalleri et al., Tracking the motion of charges in a terahertz light field by femtosecond X-ray diffraction. *Nature* **442**, 664 (2006)
22. J.-H. Kim et al., Coherent phonons in carbon nanotubes and graphene. *Chem. Phys.* **413**, 55 (2013)
23. A.V. Kuznetsov, C.J. Stanton, Theory of coherent phonon oscillations in semiconductors. *Phys. Rev. Lett.* **73**, 3242 (1994)
24. M. Kan, H.G. Nam, Y.H. Lee, Q. Sun, Phase stability and Raman vibration of the molybdenum ditelluride (MoTe₂) monolayer. *Phys. Chem. Chem. Phys.* **17**, 14866 (2015)
25. K. Gofasa et al., Resonant quenching of Raman scattering due to out-of-plane A_{1g}/A_{1'} modes in few-layer MoTe₂. *Nanophotonics* **6**(6), 1281–1288 (2017)
26. I.G. Lezama et al., Indirect-to-direct band gap crossover in few-layer MoTe₂. *Nano Lett.* **15**, 2336 (2015)
27. P. Giannozzi et al., QUANTUM ESPRESSO: a modular and open-source software project for quantum simulations of materials. *J. Phys. Condens. Matter* **21**, 395502 (2009)

Publisher's Note Springer Nature remains neutral with regard to jurisdictional claims in published maps and institutional affiliations.